



Performance Evaluation of Gesture Recognition Using Myo Armband and Gyroscope Sensors

S. M. Sarhan^{1*}, M. Z. Al-Faiz², A. M. Takhakh³

Authors affiliations:

1*) Dep. of Biomedical Eng.,
College of Engineering,
University of Warith Al-Anbiyaa,
Karbala, Iraq
st.saad.m.sarhan@wr.edu.iq

2) Dep. of Control and
Computer, College of
Information Engineering, Al-
Nahrain University, Baghdad-
Iraq
mzalfaiz12@nahrainuniv.edu.iq

3) Dep. of Mechanical Eng.,
College of Engineering, Al-
Nahrain University, Baghdad-
Iraq
ayadmurad@nahrainuniv.edu.iq

Paper History:

Received: 11th May. 2024

Revised: 12th July. 2024

Accepted: 12th Mar. 2025

Abstract

The technique of recording muscle signals is crucial in determining how effectively they can be utilized for individual benefit. This study focuses on hand movements recognized by using the Myo armband and Motion Processing Unit (MPU) 6050 sensors. Linear Discriminant Analysis (LDA), K-nearest neighbors (k-NN), and Support Vector Machine (SVM) were employed for classification. sEMG signals using the Myo armband for 7 hand gestures and 2 elbow movements were recorded from 10 healthy subjects. Results showed that SVM outperforms LDA and k-NN in accuracy in both cases, the sensor is worn once on the arm and again on the forearm. regions. The window size and choice of features significantly influence system accuracy, with SVM achieving an average accuracy of 89.84%. Besides that, the fusion of Myo Armband sensor and gyroscope sensor through OR rule makes significant enhancement in recognition accuracy with which is reached to 97.0135%. In conclusion, the Myo armband, when worn on the forearm, proves practical for hand gesture recognition, with SVM offering superior recognition accuracy. Furthermore, the combination of the Myo Armband sensor and the gyroscope sensor showed higher recognition accuracy.

Keywords: Surface Electromyography, Support Vector Machine, Linear Discriminant Analysis, k-Nearest Neighbors.

تقييم أداء التعرف على الإيماءات باستخدام السنسر العضلي و سنسر محدد الاتجاهات
سعد محمود سرحان، محمد زكي الفايز، اياد مراد الطخاخ

الخلاصة:

تعد تقنية تسجيل إشارات العضلات ضرورية لتحديد مدى إمكانية استخدامها بفعالية لتحقيق الفائدة الفردية. تركز هذه الدراسة على التعرف على حركات اليد باستخدام سوار Myo ومستشعر Motion Processing Unit (MPU) 6050. تم استخدام تحليل التمييز الخطي (LDA)، وأقرب الجيران (k-NN)، وآلة الدعم المتجهية (SVM) للتصنيف. تم تسجيل إشارات sEMG باستخدام سوار Myo لسبع حركات يد وحركتين للكوع من 10 أشخاص أصحاء. أظهرت النتائج أن SVM تفوقت على LDA و k-NN من حيث الدقة في كلتا الحالتين، سواء عند ارتداء المستشعر على الذراع أو الساعد. كما أن حجم النافذة واختيار الميزات لها تأثير كبير على دقة النظام، حيث حققت SVM متوسط دقة بلغ 89.84%. علاوة على ذلك، أدى دمج مستشعر Myo Armband ومستشعر محدد الاتجاهات باستخدام قاعدة OR إلى تحسين ملحوظ في دقة التعرف، حيث وصلت إلى 97.0135%. ختاماً، يثبت سوار Myo Armband عند ارتدائه على الساعد فعاليته في التعرف على إيماءات اليد، مع تفوق SVM في دقة التعرف. بالإضافة إلى ذلك، أظهر الجمع بين مستشعر Myo Armband ومستشعر محدد الاتجاهات زيادة في دقة التعرف.

1. Introduction

The relationship between humans and robots has garnered significant interest from the academic community, technological firms, government labs, and other sectors [1]. There are multiple muscles in the arm

and forearm that move the hand and fingers. The forearm is split into the anterior compartment and posterior compartment by the deep fascia of the forearm, which covers 13 muscles in the forearm. These compartments are frequently separated by three

barriers [2]. Three main layers make up the anterior compartment muscles: the superficial layer, middle layer, and deep layer. These muscles' primary job is to allow for the pronation of the hand, as well as wrist and finger flexion. The superficial layer and deep layer are the two main layers in which the posterior compartment muscles are located. The muscles in the posterior compartment primarily extend the fingers, with auxiliary activities including wrist extension and supination [3]. A visual-based gesture recognition system primarily uses a camera to perceive gestures. These systems frequently have many issues, including position, hand motion modelling complexity, sensitivity to light, and changing distance. However, because they rely on the muscular contraction of the hand rather than external sensor detection, hand gesture recognition systems based on internal sensor detection (such as surface electromyography (sEMG) signal) are thought to be one of the distinguishing techniques [4]. Surface electrodes and needle electrodes (into the skin) are the two primary electrode types used to capture EMG signals, and there is little difference between them [5]. Surface electrodes come in two varieties: gelled and dry sEMG electrodes [6]. Self-balancing robots use IMU sensors, such as the MPU 6050. IMU sensors are typically made up of 2 or more components. The accelerometer, gyroscope, magnetometer, and altimeter are listed in order of priority. As an IMU sensor with 6 axes and 6 degrees of freedom, the MPU 6050 provides 6 values as output: three from the gyroscope and three from the accelerometer. A sensor built using MEMS (micro electro mechanical systems) technology. A single chip contains both the gyroscope and the accelerometer. The inter-integrated circuit (I2C) protocol is used by this chip for communication. When the gyroscope and accelerometer of the MPU sensor are combined, efficiency increases. In addition, integrating the Myo Armband sensor with the MPU 6050 sensor will improve the recognition accuracy of the output [7]. The goal of this study is to integrate sensors for the purpose of overcoming the weakness in the muscles of the upper limbs and to demonstrate the possibility of relying on information whose accuracy does not depend on muscle strength.

2. EMG Signal Processing

This section describes the sEMG signal, how it is generated, and how to detect it. Additionally, the pattern recognition system is demonstrated for use in sEMG signal analysis to differentiate hand motions.

2.1. The electromyogram (EMG) signal

The amplitude, frequency, and phase of the EMG signal, which is often a function of time, can be used to define the signal. This signal, which represents neuromuscular activity, is a biological signal that can be detected as electrical signal during muscle contractions. The amplitude range of the EMG signal is 0–10 mV (± 5 mV) before amplification. As EMG signals travel through various tissues, noise is picked up [8]. The EMG frequency ranges vary based on the type of investigation from 0.01 Hz to 10 kHz (invasive or non-invasive). The frequency ranges between 50 and 150 Hz are the most crucial and beneficial [9].

2.2. Myo gesture armband

The wireless, 8-channel Myo gesture control armband is a wearable device designed primarily to detect and measure EMG signals from the muscles in the forearm as shown in Fig. 1. Thalmic Labs developed cutting-edge technology for this device. Gyroscope, accelerometer, and magnetometer are its three component pieces. All of these components, which individually have the x, y, and z axes, together comprise the Inertial Measurement Unit (IMU). It has 2 batteries inside, each of which is located in a different place and has a capacity of 260 mAh and a voltage range of 1.7 to 3.3 volts. It has a 200 Hz sampling rate [10].

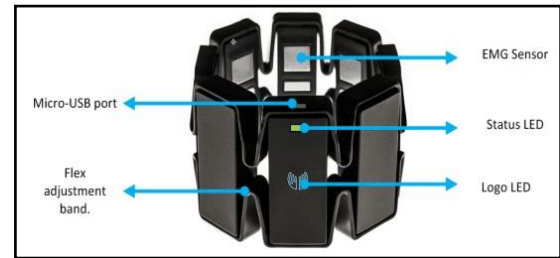


Figure (1): Myo gesture armband [11]

2.3. Pattern recognition system

Signal segmentation, feature extraction, and implementation of the appropriate classification to ascertain the new samples' class are the three fundamental building blocks of a pattern recognition method. The input raw EMG signal is segmented during the training stage of the pattern recognition algorithm, and feature extraction is used to convert each segment into a collection of features. These features gather pertinent information on each segment, which is then used to classify it [12].

2.3.1. sEMG segmentation technique

Many techniques, including the adjacent scheme, overlap scheme, and segmentation technique, are employed in the segmentation portion to cut off the sEMG signals. This study makes use of an overlapping approach. This segmentation approach divides the sEMG signals into regular time slot windows that overlap. In the overlap technique, the Classification Decision (CD) can be determined as:

$$CD = \frac{1}{2}T_a + \frac{1}{2}T_{new} + \tau \quad \dots(1)$$

where T_a is the length of the analytic window, T_{new} is the window increment, and τ is the processing time. The method is referred to as adjacent windowing when $T_{new}=T_a$ [13].

2.3.2. Feature extraction, reduction, and classification

The characteristics of amplitude and frequency information are essential for differentiating sEMG signal patterns. The amplitude and frequency-related Time Domain (TD) characteristics are helpful features [14]. Recently, scholars have been using TD features extensively to identify patterns in sEMG signals because of its cheap processing cost [15]. 6 TD features were extracted as follows:

- Root Mean Square (RMS): It possesses frequency-related characteristics that correspond to the segment's square root of



the mean square. RMS is mathematically represented as follows:

$$RMS = \sqrt{\frac{1}{N} \sum_{i=1}^N x_i^2} \quad \dots(2)$$

Where: x_i represents the sEMG signal and N denotes the sample number of the sEMG signal.

- Mean Absolute Value (MAV): It has amplitude-related characteristics that represent the computation of the segment's mean absolute value. MAV is mathematically represented as follows:

$$MAV = \frac{1}{N} \sum_{i=1}^N |x_i| \quad \dots(3)$$

- Slope Sign Changes (SSC): It possesses frequency-related properties that can count and identify shifts in the slope sign of the sEMG signal. SSC is mathematically represented as follows:

$$SSC = \sum_{n=2}^{N-1} |f[(x_n - x_{n-1})(x_n - x_{n+1})]| \quad \dots(4)$$

Where: x_{n-1} , x_n , and x_{n+1} have been used for any three successive values.

- Waveform Length (WL): It has amplitude-related features that represent the cumulative length of the sEMG waveform over the time segment. The mathematical representation of WL is as follows:

$$WL = \sum_{i=1}^{N-1} |x_{i+1} - x_i| \quad \dots (5)$$

- Zero Crossings (ZC): It has frequency-related features that count the number of signal amplitudes crossing the zero amplitude over the time segment. The mathematical representation of ZC is as follows:

$$ZC = \sum_{n=1}^{N-1} \text{sgn}(x_n x_{n+1}) \cap |x_n - x_{n+1}| \geq \text{threshold},$$

$$\text{where, } \text{sgn}(x) = \begin{cases} 1 & \text{if } x \geq \text{threshold} \\ 0 & \text{otherwise} \end{cases} \quad \dots(6)$$

- Autoregressive (AR): This is the linear combination of the error term and the previous windows. The following is how AR is represented mathematically:

$$x_k = \sum_{i=1}^p a_i x_{k-i} + e_k \quad \dots (7)$$

Where: a_i is the autoregressive coefficients, p is the model order, x_{k-i} is the sEMG sample, and e_k is the residual white noise. Features reduction is applied mainly to improve the performance of the classifier. LDA and Principal Component Analysis (PCA) are the two most popular feature reduction techniques [13]. In this study, LDA, k-NN, and SVM were investigated to determine how well they classified 2 elbow movements and 7 hand gestures based on sEMG signals.

2.3.2.1. SVM classifier

The SVM is a linear model that creates non-linear classification boundaries. It concludes a computationally efficient route of learning a "good" splitting hyperplane in dimensional feature space, whereby a "good" hyperplane could differentiate between fresh sample classes. To generalize optimal hyperplanes, there are different mathematical algorithms used depending on the data set separable

state [16]. When the situation becomes linear, SVM transforms the data nonlinearly using appropriate selection basis functions into a higher-dimensional feature space. This transformation represents the concept of implementing the kernel trick. The Radial Basis Function (RBF) kernel as in expression (8) and linear as in expression (9) were used in this work, where:

$$K(x_n, x_i) = \exp(-\gamma \|x_n - x_i\|^2) \quad \dots (8)$$

This is the RBF kernel, which measures similarity between two input vectors x_n and x_i (Non-linear). The exponential function ensures that points closer in space have higher similarity, while distant points have lower similarity.

Parameters:

- $K(x_n, x_i) \rightarrow$ Kernel function output (measuring similarity between two data points).
- $x_n, x_i \rightarrow$ Feature vectors of two data points.
- $\|x_n, x_i\|^2 \rightarrow$ Squared Euclidean distance between the two vectors.
- γ (gamma) \rightarrow Controls how much influence a single training sample has:
 - o Higher γ : More localized influence (small decision boundaries, risk of overfitting).
 - o Lower γ : More generalized influence (smooth decision boundaries, risk of under fitting).

$$K(x_n, x_i) = (\gamma x_n, \gamma x_i) \quad \dots(9)$$

- This represents a linear kernel, where the similarity between two points is calculated as a simple dot product.
- The multiplication by γ scales the feature space but does not introduce non-linearity.

Parameters:

- $K(x_n, x_i) \rightarrow$ Kernel function output (similarity measure).
- $x_n, x_i \rightarrow$ Feature vectors of two data points.
- $\gamma \rightarrow$ Scaling factor that adjusts the influence of feature values.

Let us now define two key concepts that will be used often throughout this text.

- Support vectors: are the spots nearest to the hyperplane. The data points will be used to define a separation line.
- The margin: is the distance between the hyperplane and the observations nearest to it. In SVM, a big margin is considered excellent [17].

Fig. 2, shows the basic principle of support vectors.

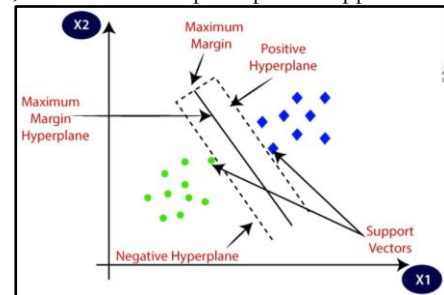


Figure (2): The support vectors[20].

2.3.2.2. LDA classifier

A new observation should be assigned to mutually exclusive groups using the LDA, a statistical classifier.

Similar to the SVM technique, the goal of LDA is to locate a hyperplane that can divide the data points into various classes. Under the premise of normal data distribution, this hyperplane can be discovered by looking for a model that increases the distance between the mean of the classes and decreases the variation within each class [18]. The LDA is based on the Bayes rule of classification. For a specifically tested vector x would be predicted to group C_k as this variance is fulfilled in the following expression

$$P(C_k | x) = \frac{P(C_k) P(x | C_k)}{P_x} \quad \dots (10)$$

Where $P(x)$ is the training space's probability density function, which is also presumed to be equal for all classes, $P(C_k)$ is the prior probability for class k and $P(x | C_k)$ is the probability density function for the test vector within the k class [17][19].

2.3.2.3. K-NN classifier

The KNN is a lazy learning and non-parametric algorithm. Non-parametric means there is no hypothesis for underlying data distribution [20]. Starting at the test point, the k-NN method expands the region until it has k training samples, then uses the majority vote of these samples to determine the test x point [13].

3. Materials and Methods









10 healthy subjects were involved in this study. Table 1 contains details about the 10 healthy participants in this investigation.







Table (1): Information on healthy subjects.

Subjects	Gender	Age	Weight (kg)	Length (cm)
Subject1	Male	44	76	170
Subject2	Male	42	81	173
Subject3	Male	41	75	165
Subject4	Male	38	72	169
Subject5	Male	25	69	160
Subject6	Male	35	73	172
Subject7	Female	34	66	165
Subject8	Female	40	74	170
Subject9	Female	39	70	164
Subject10	Female	22	61	159

A variety of subjects took part, as indicated in Table 1 above, and the Myo gesture armband was used to record all of the sEMG signals from the right hand. By placing the armband on the forearm region, 8 datasets (each containing 7 movements) were recorded for each individual, as indicated in Table 2.

Table (2): Hand gestures with properties (Myo armband on the forearm and arm).

No.	Forearm	Arm	Name	Description
1			rest	The hand is relaxed
2			close	The hand is tightly closed
3			open	The fingers are fully opened
4			left	The hand is turned to the left

5			right	The hand is turned to the right
6			up	The hand is directed upward
7			down	The hand is directed downward

Each single data set is composed of 56000 samples (7 gestures \times 8 sensors (Myo Armband composed of 8 EMG sensors) \times 5 seconds (recording time for each gesture) \times 200 samples (sampling frequency for Myo Armband=200Hz)) represented in a 7000×8 matrix as shown in Table (3). In addition, each gesture is composed of 1000 data samples and for first gesture (rest) starts from sequence 1 to 1000, the second gesture (close) starts from 1001 to 2000, and so on, whereas the 7th gesture starts from 6001 to 7000. The length of each dataset is 35 seconds because each gesture in the dataset lasts for five seconds and begins with a resting hand motion. Each subject's entire dataset recording lasts for 280 seconds.

Table (3): Matrix of channels and the movements

Channel	Ch. 1	Ch. 2	Ch. 3	Ch. 8
Sequence				
1	0	-0.00781	0	0.00231
2	0.01653	-0.01563	0	-0.00781
3	-0.00826	0	-0.00156	-0.00324
4	-0.00213	-0.02647	-0.00572	-0.00781
7000	0.01562	-0.09372	0.09750	0.39841

Using a cross-validation technique, the dataset was split into a training set (80%) and a testing set (20%). The original dataset is randomly divided into k sub-datasets of equivalent size for cross-validation. While one sub-dataset is preserved as validation data to test the model, the remaining sub-datasets are used as training sets. The recorded datasets were divided into 8 smaller datasets to execute cross-validation as shown in Fig.3. The identical hand motions were recorded once again during the recording process, which was performed for all datasets by positioning the sensor on the arm region, as indicated in Table 2. Two elbow movements (flexion and extension) also were recorded for ten subjects.

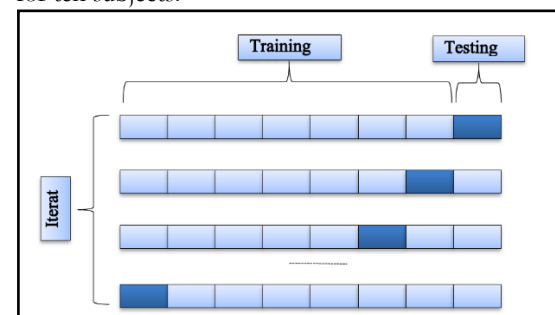


Figure (3): Cross-validation k-fold technique with $k=8$

The consequences of the motor units' firing rates on the sEMG signals cause intrinsic instability to occur. The noise ratio in sEMG signals is practically low when using the Myo gesture armband, and it has no effect on the results. Usually between 0 and 2 mV, the sEMG signal voltage is quite low. Processing, identification, and gesture selection are critical issues for the gestural interface to work well. The movements were chosen based on the existence of a large difference between them, in addition to the fact that they exert more effort than others, and thus they help in the rehabilitation process. The MPU sensor was employed to monitor the flexion and extension movements of the elbow and hand as shown in Fig.4.

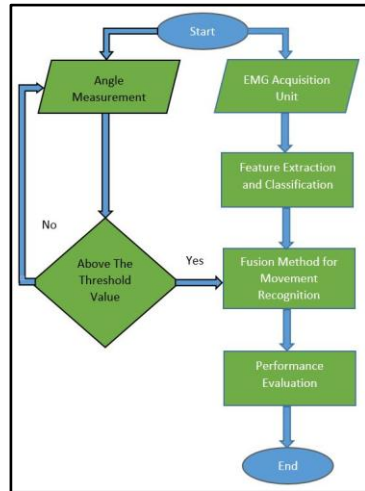


Figure (4): Flow chart of direction and muscle signal fusion method.

4. Data Processing and Analysis

The sEMG signals corresponding to 7 hand gestures from 10 subjects were immediately recorded and saved onto a personal laptop. Then, using MATLAB (Version R2020a, The MathWorks, Inc.), data processing and analysis were carried out. The generally noisy character of the obtained sEMG data is caused by ambient noise, motion artifact, intrinsic noise in electronics equipment, and inherent instability of the sEMG signal. Ambient noise is caused by electromagnetic device radiation, whereas motion artifact noise is caused by the contact between the electrode and the skin. The consequences of the motor units' firing rates on the sEMG signals cause intrinsic instability to occur. The signal-to-noise ratio in sEMG signals is essentially low when utilizing the Myo gesture armband, which has little impact on the sEMG data. Using the proposed SVM flowchart as shown in Fig. 5.

This attribute is thought to be crucial for the Myo armband. The offline mode was designed to improve system performance and calculate accuracy. The MATLAB R2020 program has been used to implement this mode. To ensure that its sensors are placed in the same locations each time it is used to record datasets, the Myo gesture armband should be worn consistently. This issue needs to be taken into account when recording data to prevent erratic readings. To compare the differences in accuracies between the two scenarios, the Myo armband is worn on the right forearm first and then the right arm in this

investigation as shown in Tables 2. To capture the flexion and extension of the elbow joint, it is also worn on the right arm as shown in Table 2. All channels of the Myo armband were used to collect the sEMG data. The data collected by the Myo armband is transferred over Bluetooth to the PC for analysis and processing in the MATLAB R2020 environment. The recorded dataset (7 movements repeated 8 times with 5 seconds for each movement) lasts for 280s. The dataset's window size is 250 ms, with a 125 ms overlap. The total number of features extracted across all sets and channels is 72, which is equal to the product of the 8 Myo channels and the 6 features (RMS, MAV, SSC, ZC, WL, and AR with order = 4) that are extracted for each window (segment). With the help of the K-NN, LDA, and SVM classifiers, the system's accuracy is calculated.

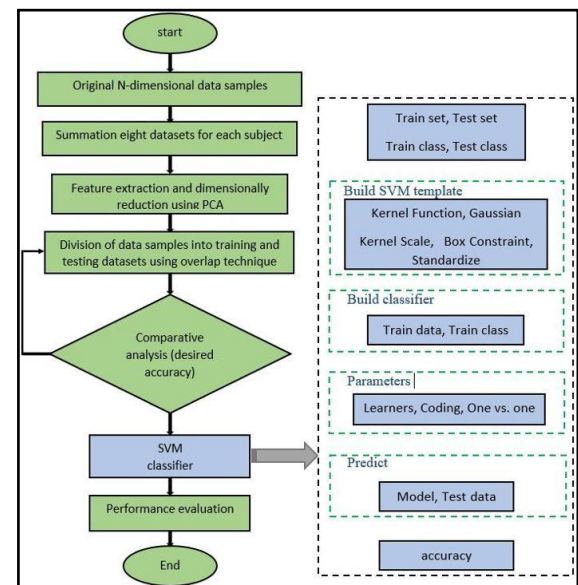


Figure (5): The proposed flowchart of the SVM algorithm.

This attribute is thought to be crucial for the Myo armband. The offline mode was designed to improve system performance and calculate accuracy. The MATLAB R2020 program has been used to implement this mode. To ensure that its sensors are placed in the same locations each time it is used to record datasets, the Myo gesture armband should be worn consistently. This issue needs to be taken into account when recording data to prevent erratic readings. To compare the differences in accuracies between the two scenarios, the Myo armband is worn on the right forearm first and then the right arm in this investigation as shown in Tables 2. To capture the flexion and extension of the elbow joint, it is also worn on the right arm as shown in Table 2. All channels of the Myo armband were used to collect the sEMG data. The data collected by the Myo armband is transferred over Bluetooth to the PC for analysis and processing in the MATLAB R2020 environment. The recorded dataset (7 movements repeated 8 times with 5 seconds for each movement) lasts for 280s. The dataset's window size is 250 ms, with a 125 ms overlap. The total number of features extracted across all sets and channels is 72, which is equal to the product of the 8

Myo channels and the 6 features (RMS, MAV, SSC, ZC, WL, and AR with order = 4) that are extracted for each window (segment). With the help of the K-NN, LDA, and SVM classifiers, the system's accuracy is calculated.

5. Results and Discussions

The findings of the studies and the variables influencing the system's accuracy are covered in this section. The duration of the window, the kind of characteristics chosen, and the classifier are determining factors.

5.1. Window length and accuracy

The window size was increased from 100 to 700 milliseconds. Through a trade-off between system accuracy and delay time, the best results were obtained when the window size was 250 ms with 125 ms overlapping because the recognition accuracy was less when the window length was 260 ms or longer and when it was 240 ms or shorter.

5.2. Extracted features and accuracy

For 10 participants, 6 features and 8 channels of Myo gesture armband were selected. ZC had the least impact on system accuracy among MAV, RMS, WL, AR, ZC, and SSC features. When compared to LDA and k-NN classifiers, SVM classifiers had the best accuracy. By integrating 2 MPU sensors and accurately measuring the angles of both the hand and elbow, we achieved improved movement discrimination compared to using the Myo Armband sensor alone.

5.3. Number of channels

Fig.6 shows the 7 hand movements by using 8 channels with 1000 samples for each movement arranged on the sequence rest, right, left, up, down, contract, and open.

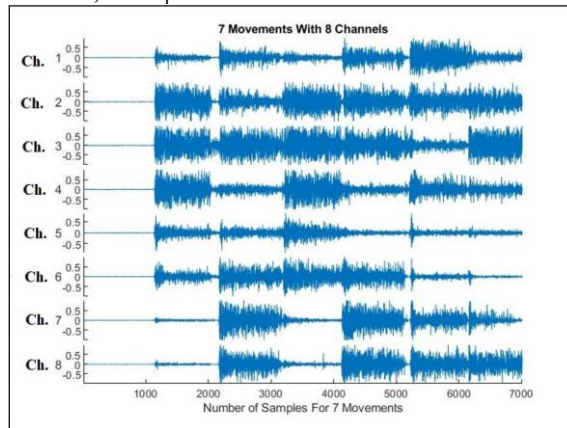


Figure (6): Raw EMG signal for 7 movements recorded with 8 channels.

According to the electrodes' locations on the forearm region, the amplitude of each sensor is different in each movement. Since Channel 5 doesn't have an impact on the classification accuracy, it can be neglected during measurement to reduce the amount of data. Table (4) shows the average recognition accuracies (%) by using 8 sensors by placing the Myo armband on the forearm region.

As shown in Table 4, the classification accuracies by using the SVM classifier were better than LDA and KNN classifiers. The same hand motions from Table 5 were used to repeat this process, and the identical

results (%) were displayed, highlighting the fact that the SVM is the most effective classifier based on these data.

Table (4): Average recognition accuracies % for forearm region

Subjects	SVM	LDA	k-NN
<i>Subject1</i>	92.8065	93.9371	83.3400
<i>Subject2</i>	89.0798	89.8538	77.3339
<i>Subject3</i>	91.8663	92.2295	71.1939
<i>Subject4</i>	93.7838	93.7162	70.4054
<i>Subject5</i>	94.2735	93.2621	68.7932
<i>Subject6</i>	92.7968	91.3848	74.5310
<i>Subject7</i>	82.5316	85.9496	65.4922
<i>Subject8</i>	75.9051	74.4740	54.9093
<i>Subject9</i>	92.3213	91.2231	88.3602
<i>Subject10</i>	93.0313	92.0021	89.4204

Table (5): Average recognition accuracies % for arm region

Subjects	SVM	LDA	k-NN
<i>Subject1</i>	66.7540	69.0033	64.691
<i>Subject2</i>	76.9116	78.9513	72.9599
<i>Subject3</i>	52.2789	49.7162	41.5500
<i>Subject4</i>	56.4238	55.6618	46.5404
<i>Subject5</i>	64.3980	62.7094	55.0517
<i>Subject6</i>	67.5652	66.9009	59.9216
<i>Subject7</i>	66.2317	66.2330	59.4407
<i>Subject8</i>	50.8350	49.3003	45.1190
<i>Subject9</i>	57.3091	48.3421	44.6824
<i>Subject10</i>	60.3401	55.3502	48.5603

From Table 4, the average SVM accuracies for 10 subjects were 89.8396% for the forearm region, and for the arm region (Table 5) were 61.9047%. The result of the forearm was better than the arm with 27.9349%. The flexion and extension were also recorded (%) by placing the sensor on the arm region as shown in Table 6 below.

Table (6): Average recognition accuracies % for flexion and extension movements.

Subjects	SVM	LDA	k-NN
<i>Subject1</i>	99.6032	99.4048	99.6002
<i>Subject2</i>	99.2034	99.0213	99.0923
<i>Subject3</i>	98.8032	98.2043	98.3902
<i>Subject4</i>	99.6377	99.1836	99.4828
<i>Subject5</i>	99.4667	99.0376	99.0184
<i>Subject6</i>	99.7489	99.3859	99.8365
<i>Subject7</i>	98.8367	99.8624	99.6425
<i>Subject8</i>	99.7326	99.5277	99.4327
<i>Subject9</i>	99.1834	99.3625	99.8265
<i>Subject10</i>	99.8460	99.73657	99.0356

From the above results, it was shown that the SVM was better than the other two classifiers. The high classification accuracy is due to 2 reasons: first, the number of movements is 2 only (flexion and extension), and second, the location of muscles responsible for these 2 movements are non-overlapping (biceps for flexion and triceps for extension). The rest movement was the best with 80



% in SVM, 70 % LDA, and 80 % k-NN, while the worst movement in SVM was the left with 40 %, right movement with 30% in LDA, and right and down movements with 30% in k-NN.

5.4. Fusion of the sensors

The integration of the muscle sensor with gyroscope sensor shows a significant improvement in the accuracy of the measured signal, as shown in the Table 7 below.

Table (7): Average recognition accuracies % for forearm region with and without fusion method.

<i>subjects</i>	<i>SVM without fusion method</i>	<i>SVM with fusion two sensors</i>
<i>Subject1</i>	92.8065	97.7589
<i>Subject2</i>	89.0798	96.5306
<i>Subject3</i>	91.8663	95.6498
<i>Subject4</i>	93.7838	98.0320
<i>Subject5</i>	94.2735	98.9555
<i>Subject6</i>	92.7968	97.9088
<i>Subject7</i>	82.5316	95.6229
<i>Subject8</i>	75.9051	94.1994
<i>Subject9</i>	92.3213	97.8240
<i>Subject10</i>	93.0313	97.6532
Average	89.8396	97.0135

From the table above, the integration was carried out using the OR rule, through which we can identify the measured signal if we receive input from either the muscle sensor or the gyroscope sensor or both. Consequently, the result is much better than using any sensor individually.

6. Conclusion

The muscle sensor can be worn on the arm or on the forearm to record hand gestures. However, when worn on the forearm, the accuracy in distinguishing hand movements is much higher compared to wearing it on the arm. The purpose is to demonstrate the potential benefit of arm signals for individuals with amputations above the elbow. The ability to recognize human forearm gestures based on sEMG signals gathered by the wireless removing channel 5 reduces processing time and data required for classification. The SVM classifier in this study showed better recognition accuracy than LDA and k-NN classifiers with and without fusion method. The results showed that the system's accuracy is significantly influenced by the window's size and increased obviously in combination two sensors through OR rule. A suggestion for further study in this area would be to gather additional information from volunteers who are both able-bodied and physically disabled to get more firm conclusions about the system's accuracy. Adding more gyroscope sensors could make the recognition ability higher.

7. Conflicts of Interest

All the researchers have agreed to prepare this research and there is no conflict of interest in completing this work.

8. Author Contributions

Saad M. Sarhan and Mohammed Z. Al-Faiz; methodology, and formal analysis, Saad M. Sarhan; software, writing—original draft preparation, and resources, Ayad M. Takhakh; validation, visualization, project administration, and funding acquisition, Mohammed Z. Al-Faiz; investigation, data curation, writing—review and editing, and supervision.

9. References

- [1] A. Hogenhuis, "Social network engagement during human-robot interaction," in Companion of the 2023 ACM/IEEE Int. Conf. on Human-Robot Interaction, Mar. 2023. DOI:10.1145/3568294.3579976
- [2] S. Hall and J. Stephens, Anatomy and Physiology. Amsterdam: Elsevier, 2019.
- [3] S. Madarshahian and M. L. Latash, "Effects of hand muscle function and dominance on intra-muscle synergies," Hum. Mov. Sci., vol. 82, p. 102936, Apr. 2022. DOI:10.1016/j.humov.2022.102936
- [4] S. Bisi, L. De Luca, B. Shrestha, Z. Yang, and V. Gandhi, "Development of an EMG-controlled mobile robot," Robotics, vol. 7, no. 3, p. 36, 2018. DOI:10.3390/robotics7030036
- [5] A. Sharma, I. Sharma, and A. Kumar, "Signal acquisition and time-frequency perspective of EMG signal-based systems and applications," IETE Tech. Rev., vol. 41, no. 4, pp. 466–485, Oct. 2023. DOI:10.1080/02564602.2023.2265897
- [6] M. A. Ozdemir, D. H. Kisa, O. Guren, and A. Akan, "Dataset for multi-channel surface electromyography (SEMG) signals of hand gestures," Data Brief, vol. 41, p. 107921, Apr. 2022. DOI:10.1016/j.dib.2022.107921
- [7] Y. Long, Z. Du, W. Wang, and W. Dong, "Development of a wearable exoskeleton rehabilitation system based on hybrid control mode," Int. J. Adv. Robot. Syst., vol. 13, no. 5, p. 172988141666484, Sep. 2016. DOI:10.1177/1729881416664847
- [8] E. L. Ting, A. Chai, and L. P. Chin, "A review on EMG signal classification and applications," Int. J. Signal Process. Syst., vol. 9, no. 1, pp. 1–6, Mar. 2022. DOI:10.18178/ijsp.10.1.1-6
- [9] S. S. Bangaru, C. Wang, and F. Aghazadeh, "Data quality and reliability assessment of wearable EMG and IMU sensor for construction activity recognition," Sensors, vol. 20, no. 18, p. 5264, Sep. 2020. DOI:10.3390/s20185264
- [10] T. S. Chu, A. Y. Chua, and E. L. Secco, "A wearable myo gesture armband controlling Sphero BB-8 robot," HighTech Innov. J., vol. 1, no. 4, pp. 179–186, 2020. DOI:10.28991/HIJ-2020-01-04-05
- [11] P. Visconti, F. Gaetani, G. A. Zappatore, and P. Primiceri, "Technical features and functionalities of myo armband: An overview on related literature and advanced applications of myoelectric armbands mainly focused on arm prostheses," Int. J. Smart Sens. Intell. Syst., vol. 11, no. 1, pp. 1–25, 2018. DOI:10.21307/ijssis-2018-005



- [12] G. Dougherty, *Pattern Recognition and Classification: An Introduction*. New York, NY: Springer, 2013. [DOI:10.1007/978-1-4614-5323-9](https://doi.org/10.1007/978-1-4614-5323-9)
- [13] H. F. Hassan, S. J. Abou-Loukh, and I. K. Ibraheem, "Teleoperated robotic arm movement using electromyography signal with wearable myo armband," *J. King Saud Univ. Eng. Sci.*, vol. 32, no. 6, pp. 378–387, 2020. [DOI:10.1016/j.jksues.2019.05.001](https://doi.org/10.1016/j.jksues.2019.05.001)
- [14] H. R. Mahmood, M. K. Hussein, and R. A. Abedraba, "Development of low-cost biosignal acquisition system for ECG, EMG, and EOG," *Wasit J. Eng. Sci.*, vol. 10, no. 3, pp. 191–202, Dec. 2022. [DOI:10.31185/ejuow.vol10.iss3.352](https://doi.org/10.31185/ejuow.vol10.iss3.352)
- [15] A. Ahmed, Y. Al Mashhadany, R. Ahmad, and F. Khaleefah, "Smart prosthetics controller types: Review," *Anbar J. Eng. Sci.*, vol. 15, no. 2, pp. 131–154, Dec. 2024. [DOI:10.37649/aengs.2024.152744.1097](https://doi.org/10.37649/aengs.2024.152744.1097)
- [16] I. L. Salim, A. S. Jalal, and O. A. Awad, "A dataset for emotion recognition for Iraqi autism individuals as a step towards EEG-based therapeutic intervention," *Iraqi J. Inf. Commun. Technol.*, vol. 7, no. 3, pp. 55–70, Dec. 2024. [DOI:10.31987/ijict.7.3.284](https://doi.org/10.31987/ijict.7.3.284)
- [17] M. Z. Al-Faiz and Z. J. Ali, "Humanoid robotic hand (HRH) based on EMG signal for amputees persons," *Int. J. Emerg. Trends Eng. Res.*, vol. 6, no. 4, pp. 19–26, 2018. [DOI:10.30534/ijeter/2018/02642018](https://doi.org/10.30534/ijeter/2018/02642018)
- [18] Y. Narayan, "HB VSEMG signal classification with time domain and frequency domain features using LDA and ANN classifier," *Mater. Today Proc.*, vol. 37, pp. 3226–3230, 2021. [DOI:10.1016/j.matpr.2020.09.091](https://doi.org/10.1016/j.matpr.2020.09.091)
- [19] A. Furui, "Evaluating classifier confidence for surface EMG pattern recognition," in *Proc. 45th Annu. Int. Conf. IEEE Eng. Med. Biol. Soc. (EMBC)*, Jul. 2023. [DOI:10.1109/EMBC40787.2023.10340977](https://doi.org/10.1109/EMBC40787.2023.10340977)
- [20] E. Ozturk Kiyak, B. Ghasemkhani, and D. Birant, "High-level K-nearest neighbors (HLKNN): A supervised machine learning model for classification analysis," *Electronics*, vol. 12, no. 18, p. 3828, Sep. 2023. [DOI:10.3390/electronics12183828](https://doi.org/10.3390/electronics12183828)